高等学校化学学报
CHEMICAL JOURNAL OF CHINESE UNIVERSITIES
研究论文

基于给/受体双重相似性“桥联”聚合物受体的侧链工程构筑高性能三元有机太阳能电池

刘苗苗[1,2], 傅梦然[1,2], 高　蝶[2], 张万鹏[1], 梁　莹[2], 何媛媛[3], 赵巧巧[1], 赵廷兴[2], 李鸿波[2], 丁自成[5], 韩艳春[4]

(1. 齐鲁工业大学(山东省科学院)绿色造纸与资源循环全国重点实验室, 济南 250353;
2. 西南科技大学材料与化学学院, 绵阳 621010;
3. 重庆大学材料科学与工程学院, 重庆 400044;
4. 中国科学院长春应用化学研究所高分子科学与技术全国重点实验室, 130022;
5. 陕西师范大学材料科学与工程学院, 西安 710119)

摘要　活性层形貌对有机太阳能电池(OSCs)的光伏性能具有决定性影响. 然而, 二元共混体系通常因不合适的相分离形貌而导致太阳能电池器件效率受限. 本文通过将苯并二噻吩(BDT)单元作为给电子基团{类似于聚[(2,6-{4,8-双[5-(2-乙基己基-3-氟)噻吩-2-基]-苯并[1,2-b∶4,5-b′]二噻吩})-交替-{5,5-[1′,3′-二-2-噻吩-5,7-双(2-乙基己基)苯并[1′,2′-c∶4′,5′-c′]二噻吩-4,8-二酮]}](D18)的给电子单元}, 与作为受体基团的(2,2′-{(2Z,2′Z)-[12,13-双(2-丁基辛基)-12,13-二氢-3,9-二壬基噻吩并[2,3]噻吩并[3,2-b]吡咯并[4,5-g]噻吩并[2,3-b]吲哚-2,10-二基]双(甲亚基)}双(3-氧代-2,3-二氢-1*H*-茚-2,1-二亚基))二丙二腈(Y6)衍生物相结合, 设计合成了两种“桥接”型聚合物受体(PAs), 即苯并二噻吩-(2-乙基己基)氧基(BDT-C_2C_4)和苯并二噻吩-辛氧基(BDT-C_8), 对应BDT单元上的侧链分别为(2-乙基己基)氧基和辛氧基侧链. 这两种聚合物受体与给体D18、受体2,2′-((2Z,2′Z)-{[12,13-双(2-丁基辛基)-3,9-二壬基-12,13-二氢-[1,2,5]噻二唑并[3,4-e]噻吩并[2",3"∶4′,5′]噻吩并[2′,3′∶4,5]吡咯并[3,2-g]噻吩并[2′,3′∶4,5]噻吩并[3,2-b]吲哚-2,10-二基]双(甲亚基)}双(5,6-二氟-3-氧代-2,3-二氢-1*H*-茚-2,1-二亚基))二丙二腈(N3)呈现出互补的吸收光谱和梯度能级结构, 其中BDT-C_8与D18、N3的相容性优于BDT-C_2C_4. 当将两种PAs作为第三组分加入至D18∶N3混合体系时, 活性层形貌均得到显著改善. 其中D18∶N3∶BDT-C_8三元共混体系表现出显著优化的形貌特征, 即相分离尺度更小, 并形成纤维状网络结构. 最终, 基于D18∶N3∶BDT-C_8构筑的器件实现了18.18%的功率转化效率, 显著高于二元器件(约17.37%). 本文提出了一种相容剂策略来优化三元有机太阳能电池的共混形貌和光伏性能, 能有效减小活性层的相分离形貌, 提高器件效率.

关键词　有机太阳能电池; 三元策略; 聚合物受体; 活性层形貌

中图分类号　O631.2　　**文献标志码**　A　　doi: 10.7503/cjcu20250324

收稿日期: 2025-10-31. 网络首发日期: 2026-01-05.

联系人简介: 赵巧巧, 女, 博士, 副教授, 主要从事有机光伏薄膜微结构与性能调控方面的研究. E-mail: 18766192180@163.com
赵廷兴, 男, 博士, 副教授, 主要从事有机光伏材料的设计与合成方面的研究. E-mail: tingxingzhao@swust.edu.cn
韩艳春, 女, 博士, 研究员, 主要从事共轭聚合物薄膜形态结构与功能构效关系方面的研究. E-mail: ychan@ciac.ac.cn

基金项目: 山东省自然科学基金(批准号: ZR2022QE135)、国家自然科学基金(批准号: 52203024)、山东省高等学校“青创团队计划”(批准号: 2023KJ330)、全国重点实验室建设重大科研专项(批准号: 2025ZDGZ02)、西南科技大学博士基金(批准号: 22zx7129)及四川省自然科学基金(批准号: 2024NSFSC2006)资助.

Supported by the Shandong Provincial Natural Science Foundation, China(No.ZR2022QE135), the National Natural Science Foundation of China (No. 52203024), the Youth Innovation Team Project of Shandong Provincial University, China(No. 2023KJ330), the Major Scientific Research Project for the Construction of State Key Lab, China(No. 2025ZDGZ02), the Doctoral Research Foundation of SWUST, China(No. 22zx7129) and the Natural Science Foundation of Sichuan Province of China(No.2024NSFSC2006).

高等学校化学学报
CHEMICAL JOURNAL OF CHINESE UNIVERSITIES
研究论文

Side-chain Engineering of "Bridging" Polymer Acceptors with Donor/Acceptor Dual Similarity for High-performance Ternary Organic Solar Cells

LIU Miaomiao[1,2], FU Mengran[1,2], GAO Die[2], ZHANG Wanpeng[1], LIANG Ying[2], HE Yuanyuan[3], ZHAO Qiaoqiao[1*], ZHAO Tingxing[2*], LI Hongbo[2], DING Zicheng[5], HAN Yanchun[4*]

(*1. State Key Laboratory of Green Papermaking and Resource Recycling, Qilu University of Technology, Shandong Academy of Sciences, Jinan* 250353, *China*;
2. School of Materials and Chemistry, Southwest University of Science and Technology, Mianyang 621010, *China*;
3. College of Materials Science and Engineering, Chongqing University, Chongqing 400044, *China*;
4. State Key Laboratory of Polymer Science and Technology, Changchun Institute of Applied Chemistry, Chinese Academy of Sciences, Changchun 130022, *China*;
5. School of Materials Science and Engineering, Shaanxi Normal University, Xi'an 710119, *China*)

Abstract The morphology of active layer plays a critical role in determining the photovoltaic performance of organic solar cells(OSCs). However, binary blends often suffer from suboptimal phase separation, which limits the efficiency of OSCs. Herein, two bridging polymer acceptors(PAs)——benzodithiophene-(2-ethylhexyl)oxy(BDT-C_2C_4) and benzodithiophene-octyloxy(BDT-C_8)——are designed and synthesized by combining a benzodithiophene(BDT) unit as the donor moiety[poly({4,8-bis[5-(2-ethylhexyl)-4-fluorothiophen-2-yl]benzo[1,2-b:4,5-b′]dithiophene-2,6-diyl})[5,8-bis[4-(2-butyloctyl)thiophen-2-yl]dithieno[3′,2′:3,4]}, D18], and a 2,2′-((2Z,2′Z)-{[12,13-Bis(2-butyloctyl)-12,13-dihydro-3,9-dinonylthieno[2,3]thieno[3,2-*b*]pyrrolo[4,5-*g*]thieno[2,3-*b*]indole-2,10-diyl]bis(methanylylidene)}bis(3-oxo-2,3-dihydro-1*H*-indene-2,1-diylidene))dimalononitrile(Y6) derivative as the acceptor moiety. BDT-C_2C_4 and BDT-C_8 are functionalized with (2-ethylhexyl)oxy and octyloxy side chains on the BDT unit, respectively. Both PAs show complementary absorption and cascaded energy levels with the donor D18 and the acceptor 2,2′-((2Z,2′Z)-{[12,13-bis(3-ethylheptyl)-3,9-diundecyl-12,13-dihydro-[1,2,5]thiadiazolo[3,4-e]thieno[2″,3″:4′,5′]thieno[2′,3′:4,5]pyrrolo[3,2-*g*]thieno[2′,3′:4,5]thieno[3,2-*b*]indole-2,10-diyl]bis(methaneylylidene)}bis(5,6-difluoro-3-oxo-2,3-dihydro-1*H*-indene-2,1-diylidene))dimalononitrile(N3), but BDT-C_8 exhibits better compatibility with D18 and N3 compared to BDT-C_2C_4. When incorporated as a third component into the D18∶N3 blend, both PAs improve the active layer morphology. In particular, the D18∶N3∶BDT-C_8 blend shows significantly optimized morphology, featuring reduced phase separation and a fibrous network structure. As a result, the device based on D18∶N3∶BDT-C_8 achieves a power conversion efficiency of 18.18%, significantly higher than that of the device based on D18∶N3(*ca.*17.37%). This work presents a compatibilizer strategy for optimizing blend morphology towards high-performance ternary OSCs.

Keywords Organic solar cell; Ternary strategy; Polymer acceptor; Active layer morphology

1 Introduction

Organic solar cells(OSCs) have received significant attention as a promising photovoltaic technology, especially for the Internet of Things(IoT) devices, building integrated photovoltaics, portable and wearable electronic devices, due to their low cost, light weight, solution processability, and flexibility[1—11]. However, their power conversion efficiency(PCE) still needs improvement compared to silicon-based solar cells, which are widely used commercially[12—15]. At present, the typical combination of active layer materials in high-performance OSCs is usually a polymer donor(PD) and a small molecule acceptor(SMA), which has great potential for realizing high photoelectric conversion[16—19]. Nonetheless, in this system, the morphology control

of the active layer is particularly challenging. In the absence of any post-treatment, the weak intermolecular interactions and different stacking degrees between polymer donors and small molecule acceptors usually lead to unfavorable phase separation[20—25], which hinders the dissociation of excitons and the effective charge transport in the active layer. Ultimately, the photovoltaic performance is restricted in the OSC devices.

To solve this challenge, numerous morphology manipulation ways have been exploited, including solvent vapor annealing, vapor phase deposition and adding ternary component, etc[26—31]. Among them, the ternary strategy is the most fundamental approach, due to its ability to optimize the active layer morphology without complicating the device fabrication process or increasing the active layer's thickness[32—35]. However, when using the ternary strategy to optimize the morphology, the third component must be rationally selected. Compared with SMAs, polymer acceptors offer better film formation uniformity and potentially superior inter-domain connectivity[36,37]. Huang *et al.*[22] added the polymer acceptor 2,2′-((2Z,2′Z)-{[12,13-bis(2-ethylhexyl)-3,9-diundecyl-12,13-dihydro-[1,2,5]thiadiazolo[3,4-e]thieno[2″,3″:4′,5′]thieno[2′,3′:4,5]pyrrolo[3,2-g]thieno[2′,3′:4,5]thieno[3,2-b]indole-2,10-diyl]bis(methanylylidene)}bis(5,6-difluoro-3-oxo-2,3-dihydro-1*H*-indene-2,1-diylidene))dimalononitrile(PY-TPT) as the third component to the D18:L8-BO system. The resulting ternary blend film exhibited significant morphology of the double fibrillary network, and an enhanced dielectric constant, which improved exciton dissociation and charge transport, leading to a PCE of 18.60%. Zhang *et al.*[20] introduced the polymer acceptor PY-DT as a nucleating agent into the D18:L8-BO system to promote the ordered packing of L8-BO and guide its phase epitaxial growth, generated a continuous fiber network within the acceptor phase, and the PCE reached 20.3%. Zhu *et al.*[21] demonstrated that both the photovoltaic performance and mechanical properties could be improved by incorporating a polymer acceptor poly[(2,6-{4,8-bis[5-(2-ethylhexyl-3-fluoro)thiophen-2-yl]-benzo[1,2-b:4,5-b′]dithiophene})-alt-{5,5-[1′,3′-di-2-thienyl-5′,7′-bis(2-ethylhexyl)benzo[1′,2′-c:4′,5′-c′]dithiophene-4,8-dione]}](PYSe2F-T) as a ternary guest into the binary PM6:mPh4F-TT system in comparison to that adding a small-molecule ternary guest mPh4F-TS. Hence, the development of polymer acceptor as the ternary component with a simple synthesis process and high performance has emerged as a preferred alternative to optimize the morphology and realize high PCE.

In this work, two bridging polymer acceptors (PAs), benzodithiophene-(2-ethylhexyl)oxy (BDT-C_2C_4) and benzodithiophene-octyloxy (BDT-C_8), were synthesized *via* Stille coupling of a benzodithiophene (BDT) tin reagents [poly({4,8-bis[5-(2-ethylhexyl)-4-fluorothiophen-2-yl]benzo[1,2-b:4,5-b′]dithiophene-2,6-diyl})-{5,8-bis[4-(2-butyloctyl)thiophen-2-yl]dithieno[3′,2′:3,4]}, D18], and a 2,2′-((2Z,2′Z)-{[12,13-Bis(2-butyloctyl)-12,13-dihydro-3,9-dinonylthieno[2,3]thieno[3,2-*b*]pyrrolo[4,5-*g*]thieno[2,3-*b*]indole-2,10-diyl]bis(methanylylidene)}bis(3-oxo-2,3-dihydro-1*H*-indene-2,1-diylidene))dimalononitrile(Y6) bromide derivative. Meanwhile, by coordinating and regulating the side chain engineering, *i.e.*, (2-ethylhexyl)oxy and octyloxy for BDT-C_2C_4 and BDT-C_8, respectively, the molecular crystallinity and solubility, as well as the compatibility with donor and acceptor, were adjusted. The ultraviolet-visible (UV-Vis) absorptions demonstrated that BDT-C_2C_4 and BDT-C_8 possessed very similar absorption features between 400—900 nm in both chloroform solution and film state. By cyclic voltammetry (CV) testing, the HOMO/LUMO energy levels for BDT-C_2C_4 were −5.53/−3.74 eV, and −5.50/−3.70 eV for BDT-C_8. Based on complementary absorption and good energy level alignment, BDT-C_2C_4 and BDT-C_8 were incorporated as a third component into the high-performance D18:N3 binary system in the subsequent solar cell experiments. Due to the structural specialties, the PAs BDT-C_2C_4 and BDT-C_8 displayed good compatibility with both donor D18 and acceptor 2,2′-((2Z,2′Z)-{[12,13-bis(3-ethylheptyl)-3,9-diundecyl-12,13-dihydro-[1,2,5]thiadiazolo[3,4-*e*]thieno-[2″,3″:4′,5′]thieno[2′,3′:4,5]pyrrolo[3,2-*g*]thieno[2′,3′:4,5]thieno[3,2-*b*]indole-2,10-diyl]bis-

(methaneylylidene)} bis(5,6-difluoro-3-oxo-2,3-dihydro-1*H*-indene-2,1-diylidene)) dimalononitrile (N3). Through systematical device optimization, compared with the device based on the binary system of D18∶N3 with the PCE of 17.37%, the device based on D18∶N3∶BDT-C_8 blend with optimal phase separation achieved an optimal PCE of 18.18%, due to significant improvement of photon utilization, charge mobility, carrier extraction rate and lifetime. This work demonstrated that adding a compatibilizer polymer acceptor containing a similar structure to both host donor and acceptor could effectively optimize the active layer morphology and elevate the PCE of OSCs.

2 Experimental

2.1 Reagents and Instruments

Chloroform, analytical pure, Kermel Chemical Reagents Co., Ltd., China; methanol, analytical pure, Sigma-Aldrich (Shanghai) Trading Co., Ltd.; poly(3,4-ethylenedioxythiophene)(PEDOT)∶poly(styrenesulfonate)(PSS), N/A, Heraeus Group in Germany; N3, 98% purity, Shenzhen Derthon Optoelectronics Materials Sicence Technology Co., Ltd.; D18, N/A, Shenzhen Derthon Optoelectronics Materials Sicence Technology Co., Ltd.; *N*,*N*′-bis{4-[3-(dimethylamino)-1-oxopropyl]phenyl}-3,4,9,10-perylenediimide(PDINN), 99% purity, Beijing Organtec Technology Co., Ltd.; {4,8-bis[(2-ethylhexyl)oxy]benzo[1,2-b∶4,5-b′]dithiophene-2,6-diyl} bis(trimethylstannane) (Compound **1**), {4,8-bis(octyloxy)benzo[1,2-b∶4,5-b′]-dithiophene-2,6-diyl} bis(trimethylstannane) (Compound **2**) and Y6-OD-2Br, 98% purity, Zhengzhou Alpha Chemical Co., Ltd., CNC Ultrasonic Cleaner, KQ-300DE, Kunshan Ultrasound Instrument Co., Ltd.; Electronic balance, MTB2000D-B, Shenzhen Mobil Electronics Co., Ltd.; Super purifying glove box, Universal, Shanghai Michelona Electromechanical Technology Co., Ltd.; U/O ultraviolet ozone cleaning instrument, SC-UV-I, Beijing Side Case Electronics Co., Ltd.; Uniformizer(spin coater), KW-4A, Beijing Side Case Electronics Co., Ltd.; Uniformizer(spin coater), EZ4-S, Shanghai Laibo Biological Group Co., Ltd.; UV-Vis spectrophotometer, Q-6, Shanghai Yuanxi Instrument Co., Ltd.; automatic ultra-high resolution ion sputter coater, VZB-400, Beijing Micro Nano Vacuum Technology Co., Ltd.; digital electron source table, Keithley 2400, Tektronix Technology Co., Ltd.; Quantum efficiency measurement system, QE-R, Zhuhai Guangyan Technology Co., Ltd.; Class 150W Solar Simulator, XES-50S2, Japan Sanei Electric Manufacturing Co., Ltd.; High-temperature Gel Permeation Chromatograph, Agilent-1260 Infinity II, Agilent Technologies, America; Electrochemical analyzer, CHI760E, Shanghai Chenhua Instrument Co., Ltd.; contact angle analyzer, OCA50, Germany Dataphysics; automated testing platform, Paios 4.0, Switzerland Fluxim; transmission electron microscope(TEM), JEM 2100, JEOL Ltd., Japan; transient and steady-state fluorescence spectrometer, FS5, Edinburgh, UK.

2.2 Material Synthesis and Characterization

The synthetic routes of the two Bridging PAs, BDT-C_2C_4 and BDT-C_8, are shown in Scheme S1(see the Supporting Information of this paper). The detailed synthetic procedure is also shown in the Supporting Information. The high-temperature gel permeation chromatography(HT-GPC) measurement was carried out with 1,2,4-trichlorobenzene as the eluent at 150 ℃ to obtain the molecular weights of the polymers.

The UV-Vis absorption spectroscopy was tested using the Q-6 UV-Vis spectrophotometer from Shanghai Yuanxi Instrument Co., Ltd. The density functional theory(DFT) calculation was performed using Gaussian 09 software, with the functional of B3LYP and the basis set of 6-311G to probe their optimal configuration and theoretical energy levels. Cyclic voltammetry(CV) measurement was carried out using a CHI760E electrochemical analyzer to determine the electrochemical energy levels. The contact angles of donors/accepters were measured using a contact angle analyzer(OCA50), and the surface energy of materials was calculated by the

Owens-Wendt method. The details of the calculation methods are shown in the Supporting Information of this paper.

2.3 Device Fabrication and Measurements

The indium tin oxide (ITO) glass substrates were ultrasonically cleaned in detergent, deionized water, acetone, and ethanol in sequence. They were cleaned twice in detergent and deionized water for 10 min each time, then cleaned with acetone and ethanol for 15 min, respectively. After cleaning, the substrates were dried in an 80 ℃ oven. Next, the cleaned ITO substrates were ozone-cleaned for 20 min. The PEDOT∶PSS solution was spin-coated onto the substrate at a speed of 5000 r/min for 30 s, followed by thermal annealing (150 ℃, 15 min). After that, the glass substrates were transferred to a glove box. The active layer was dissolved in chloroform at a concentration of 11.13 mg/mL[m(D18)∶m(N3)=1∶1.1, with 10%(mass ratio) of BDT-C_2C_4 or BDT-C_8 added to the D18/N3 mixture], and spin-coated at 3500 r/min for 30 s. Subsequently, a methanol solution of PDINN(1.5 mg/mL) was spin-coated onto the active layer at 3000 r/min for 30 s. Finally, a 100 nm silver layer was evaporated under the vacuum of 1×10^{-4} Pa. The photoactive area used for OSC measurements was 0.045 cm^2.

The current density-voltage (J-V) characteristics were measured using a Keithley 2400 digital electron source table under AM 1.5G illumination with an intensity of 100 mW/cm^2 (XES-50S2, Japan Sanei Electric Manufacturing Co., Ltd.), calibrated with a certified standard silicon solar cell. The external quantum efficiency (EQE) spectrum was obtained through EQE testing. The hole mobility and electron mobility of the blended film were calculated using the Space-charge limited current (SCLC) method; the detailed information of testing and calculation is shown in the Support Information of this paper. The detailed information on transient photovoltage (TPV) and transient photocurrent (TPC) measurements is shown in the Support Information of this paper. The Photoluminescence (PL) spectra were tested with an excitation wavelength of 520 nm.

3 Results and Discussion

3.1 Physical and Chemical Properties

The chemical structures of the two "bridging" PAs, BDT-C2C4 and BDT-C8, polymer donor D18, and SMA N3 are shown in Fig.1(A). The side chains on the BDT unit for BDT-C_2C_4 and BDT-C_8 are (2-ethylhexyl)oxy and octyloxy, respectively. The average molecular weights and polydispersity indexes (PDIs) were 8930/1.53 and 9140/1.66 for BDT-C_2C_4 and BDT-C_8 as measured by the high-temperature gel permeation chromatography (Fig.S1, see the Supporting Information of this paper). Both of the two polymers showed excellent solubility in chloroform solution. Meanwhile, the low PDI indicated that the molecular weight distribution of PA was relatively concentrated.

The UV-Vis absorption spectra indicated that BDT-C_2C_4 and BDT-C_8 exhibited very similar absorption features between 400—900 nm in both chloroform solution (Fig.S2, see the Supporting Information of this paper) and film state [Fig.1(B)]. The maximum absorption peaks of BDT-C_2C_4 and BDT-C_8 thin films are located at 789 and 791 nm (Table S1, see the Supporting Information of this paper), respectively. While D18 exhibited significant light absorption in the range of 450—600 nm, the absorption of N3 was primarily centered in the range of 650—900 nm, with the maximum absorption peak at 822 nm. The addition of new PAs, BDT-C_2C_4 and BDT-C_8 enhanced the light absorption of the active layer [Fig.1(C)], and the absorption gap between D18 and N3 may also be compensated to some extent. According to the cyclic voltammetry (CV) results [Fig.1(D) and Fig.S3 (see the Supporting Information of this paper)], the highest occupied molecular orbital (HOMO) and lowest unoccupied molecular orbital (LUMO) energy levels of BDT-C_2C_4 and BDT-C_8 were measured to be −5.53/−3.74 eV and −5.50/−3.70 eV, respectively, which were in consistent with the DFT

calculations (the HOMO/LUMO energy levels of BDT-C_2C_4 and BDT-C_8 were −5.59/−4.58 eV and −5.53/−4.53 eV, respectively) (Fig.S4, see the Supporting Information of this paper). In comparison, D18 and N3 exhibited HOMO/LUMO energy levels of −5.52/−3.45 eV and −5.63/−3.89 eV, respectively, and the results from DFT calculation were −5.64/−2.99 eV and −6.02/−4.00 eV, respectively. The LUMO energy levels of both PAs were higher than that of N3, resulting in an increased offset relative to the HOMO energy level of the donor D18 that may improve open-circuit voltage (V_{OC}) in the OSC device. Moreover, the LUMO energy levels of PAs were located between those of D18 and N3, forming a cascade alignment that may facilitate the charge transfer. Based on complementary absorption and good energy level alignment with D18 and N3, BDT-C_2C_4 and BDT-C_8 are expected to improve the performance of D18∶N3-based OSC as a third component.

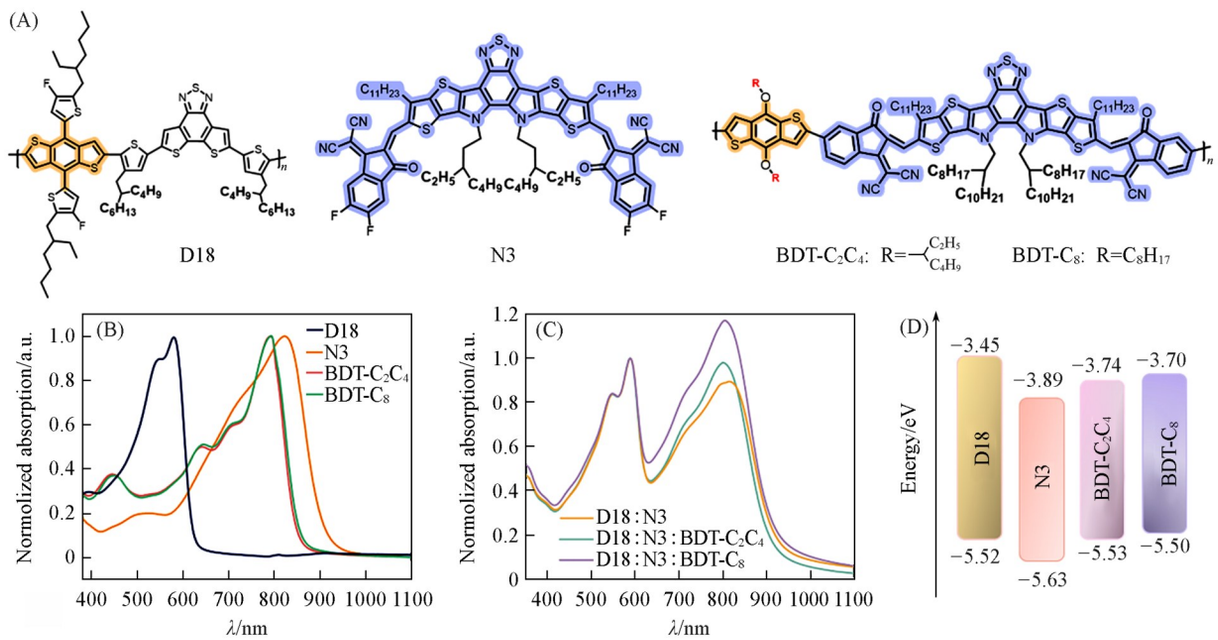

Fig. 1 Chemical structures of D18, N3, BDT-C_2C_4 and BDT-C_8(A), the normalized UV-Vis absorption spectra of neat film(B) and blend film(C), and energy levels of D18, N3, BDT-C_2C_4 and BDT-C_8(D)

3.2 Active Layer Morphology

The compatibility of the third component with the primary donor/acceptor is crucial to the morphology of the ternary blend film. To evaluate the compatibility, the contact angle test was performed with deionized water and ethylene glycol (EG), and the images and the relevant parameters are shown in Fig.2(A) and (B) and Table S2 (see the Supporting Information of this paper), respectively. According to the results, the surface energy of each component in the thin film state was calculated by the Owens-Wendt method[38,39]. The determined surface energy values of D18, N3, BDT-C_2C_4, and BDT-C_8 were 20.6, 22.6, 25.2, and 23.0 mN/m, respectively. In addition, the Flory-Huggins interaction parameter (χ) was used to evaluate the compatibility between the components, and the formula was as follows[38,40]

$$\chi_{A\text{-}B}=\kappa(\sqrt{\gamma_A}-\sqrt{\gamma_B})^2 \quad (1)$$

where κ is a parameter, γ_A (mN/m) and γ_B (mN/m) are the surface energies obtained from contact angle measurements. As a result, the χ values of BDT-C_2C_4/D18, BDT-C_8/D18, BDT-C_2C_4/N3 and BDT-C_8/N3 were 0.232κ, 0.066κ, 0.071κ and 0.002κ, respectively [Fig.2(C)]. It can be seen that both polymer guest acceptors BDT-C_2C_4 and BDT-C_8 showed good compatibility with the donor D18 and primary acceptor N3, which may alleviate the phase separation in the active layer. The smallest χ value between BDT-C_8 and D18/N3 revealed that BDT-C_8 had the best compatibility with D18 and N3, and it was also confirmed by

subsequent TEM tests, which showed that the D18∶N3∶BDT-C_8 ternary thin film displayed the smallest phase separation domain size in the ternary blend films.

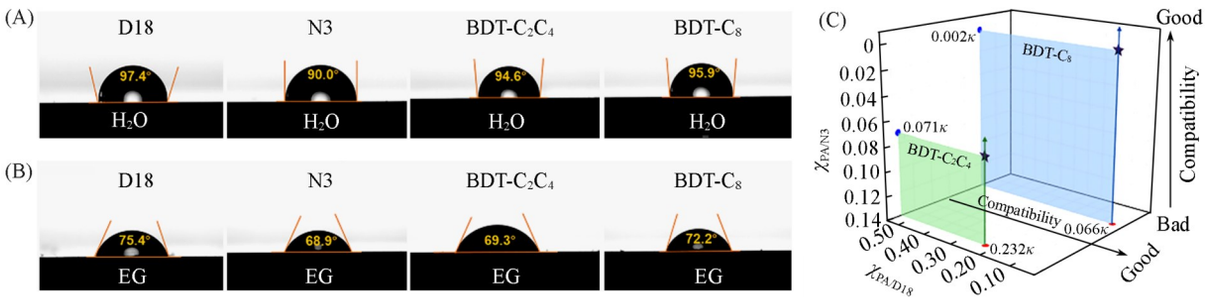

Fig. 2 Contact angles of water(A) and ethylene glycol(B) on the surface of D18, N3, BDT-C_2C_4 and BDT-C_8 films and the Flory-Huggins interaction parameter between PAs and D18/N3(C)

To investigate the influence of PAs BDT-C_2C_4 and BDT-C_8 on the morphology of the active layers, TEM observation was carried out. In the TEM images (Fig. 3), the blend film of D18∶N3 exhibited a large phase separation size. However, with the incorporation of BDT-C_2C_4 and BDT-C_8, the phase separation scale gradually decreased, especially the ternary blend film of D18∶N3∶BDT-C_8 showed the most homogeneous phase separation, which was consistent with the prediction of χ values as discussed above. In both ternary blend films, the fibrous morphologies could be observed, which were conducive to the charge transport. The moderate phase separation scale and fibrillar network structure could ensure that excitons efficiently diffuse to the donor/acceptor interface and consequently dissociate into hole and electron. As shown in Fig.S5 (see the Supporting Information of this paper), steady-state photoluminescence (PL) spectra were used to characterize the diffusion of excitons to the donor/acceptor interface. Compared with the pure film of D18, the fluorescence signal of D18 in the blend film was strongly attenuated. Meanwhile, the fluorescence intensity of D18 in the ternary blend film was significantly lower than that in the D18∶N3 binary blend film. The ternary blend film D18∶N3∶BDT-C_8 displayed the lowest fluorescence intensity, which was consistent with the suppositions from TEM that excitons could more efficiently diffuse to the donor/acceptor interface and consequently dissociate into hole and electron in the ternary blend films, especially the ternary blend film of D18∶N3∶BDT-C_8.

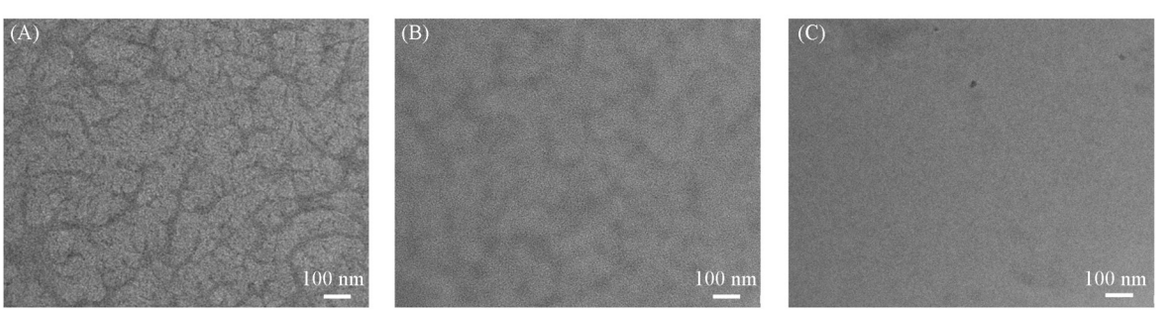

Fig. 3 TEM images of D18∶N3(A), D18∶N3∶BDT-C_2C_4(B), and D18∶N3∶BDT-C_8 blend films(C)

3.3 Photovoltaic Performance

To investigate the impact of morphology on photovoltaic efficiency, the binary and ternary devices were fabricated using the conventional ITO/PEDOT∶PSS/active layer/PDINN/Ag structure [Fig. 4(A)]. The *J*-*V* characteristics of the optimal binary and ternary devices under an AM 1.5G solar illumination are shown in Fig. 4(B), and the relevant photovoltaic parameters are summarized in Table 1. The D18∶N3 binary device showed a V_{OC} of 0.833 V, a short-circuit current density (J_{SC}, mA/cm^2) of 27.39 mA/cm^2, and a fill factor (FF, %) of 76.20%, corresponding to a moderate PCE of 17.37%. Compared with the D18∶N3 binary

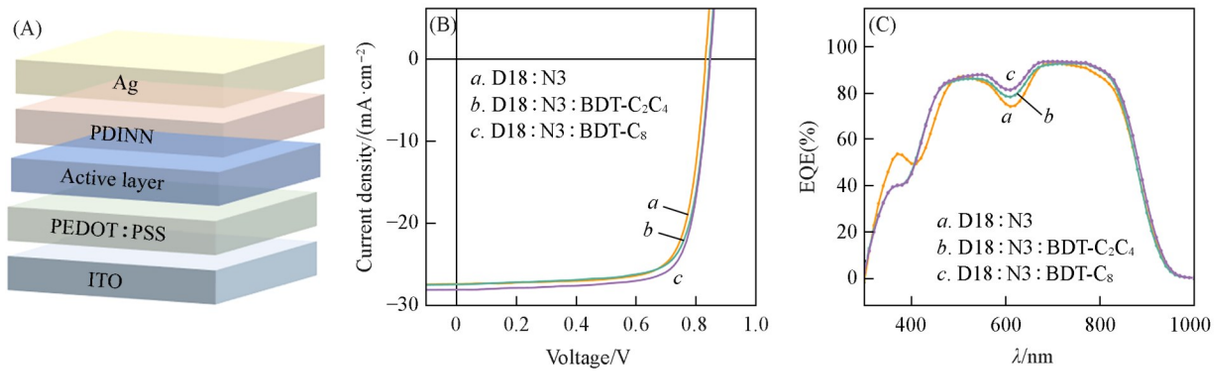

Fig. 4 Diagram of a conventional OSC device structure(A), *J-V* curves(B), and EQE curves(C) of the OSCs based on different active layers

Table 1 Photovoltaic parameters of the OSCs based on different active layers

Active layer	V_{oc}/V	J_{sc}/(mA·cm^{-2})	J^*_{cal}/(mA·cm^{-2})	FF(%)	PCE(%)
D18:N3	0.833	27.39	26.84	76.20	17.37
D18:N3:BDT-C_2C_4	0.846	27.46	27.32	75.75	17.60
D18:N3:BDT-C_8	0.849	28.08	27.92	76.25	18.18

* Integrated current densities from EQE curves.

device, both of the ternary devices showed improved V_{OC} and J_{SC}. For the device based on D18:N3:BDT-C_2C_4, the V_{OC} was increased to 0.846 V, the J_{SC} was increased to 27.46 mA/cm^2, the FF value slightly decreased to 75.75, and the final PCE was 17.60%. Delightfully, after adding BDT-C_8, the V_{OC} increased from 0.833 to 0.849 V, and J_{SC} increased from 27.39 to 28.08 mA/cm^2, resulting in an improved PCE of 18.18%. The larger V_{OC} may be due to the improved energy level alignment. The external quantum efficiency (EQE) curves of the three devices are shown in Fig.4(C). The D18:N3:BDT-C_8-based device showed higher response from 500 to 800 nm in comparison to the binary device. The J_{SC} values calculated from the EQE curves for D18:N3, D18:N3:BDT-C_2C_4, and D18:N3:BDT-C_8 based devices were 26.84, 27.32, and 27.92 mA/cm^2, which agreed well with the values obtained from the *J-V* curves, with the error less than 5%.

To explore the change of J_{SC} and FF values after the addition of PAs, the charge dynamics of the devices were investigated. The charge transport behaviors were evaluated by using the space charge limiting current (SCLC) method. As shown in Figs.5(A) and (B), the hole mobilities (μ_h, cm^2·V^{-1}·s^{-1})/electron mobilities (μ_e, cm^2·V^{-1}·s^{-1}) of devices based on the D18:N3, D18:N3:BDT-C_2C_4, and D18:N3:BDT-C_8 blend films

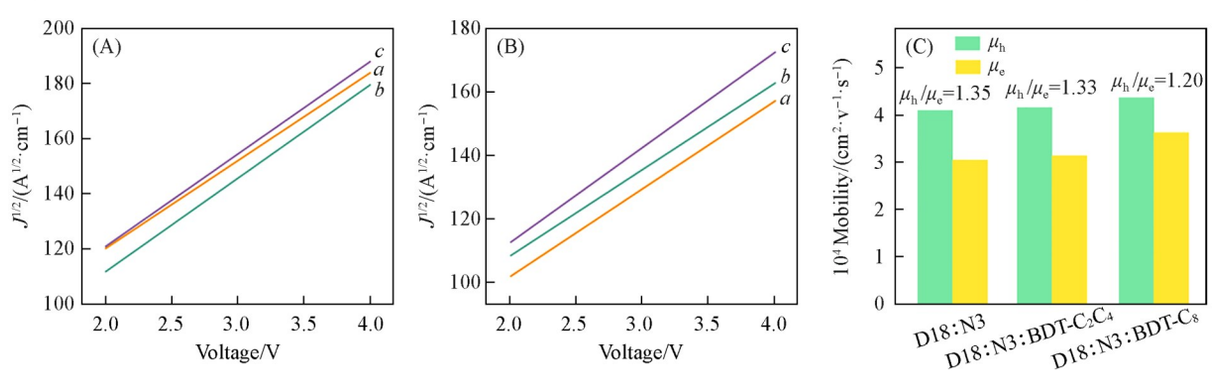

Fig. 5 Hole-only(A) and electron-only mobilities(B) of the different active layers measured using the SCLC method, and comparison of the hole and electron mobilities and their ratios in different active layers(C)

a. D18:N3; *b*. D18:N3:BDT-C_2C_4; *c*. D18:N3:BDT-C_8.

were $4.10\times10^{-4}/3.05\times10^{-4}$, $4.16\times10^{-4}/3.14\times10^{-4}$, and $4.37\times10^{-4}/3.63\times10^{-4}$ $cm^2\cdot V^{-1}\cdot s^{-1}$, respectively. Consequently, the μ_h/μ_e ratio values for D18∶N3, D18∶N3∶BDT-C_2C_4, and D18∶N3∶BDT-C_8 were determined to be 1.35, 1.33, and 1.20[Fig.5(C)], respectively. The results demonstrated that the charge transport in the D18∶N3∶BDT-C_8-based device was the fastest and the most balanced, which played a crucial role in enhancing the J_{SC} and FF.

The transient photocurrent (TPC) and transient photovoltage (TPV) tests were conducted to further explore the charge extraction and exciton diffusion processes within different devices and the results are shown in Fig.6. The charge extraction times of the D18∶N3, D18∶N3∶BDT-C_2C_4, and D18∶N3∶BDT-C_8 based devices were 0.43, 0.43, and 0.38 μs, respectively, and the carrier lifetimes were 3.26, 3.52, and 4.25 μs, respectively. Compared with the binary device, the charge extraction time of the ternary device based on D18∶N3∶BDT-C_2C_4 was not accelerated, but its carrier lifetime became longer, which may be one of the reasons for the improvement of J_{SC}. Meanwhile, the ternary device based on D18∶N3∶BDT-C_8 blend film had the shortest charge extraction time and the longest carrier lifetime, which is contributed to the enhanced J_{SC} and FF values.

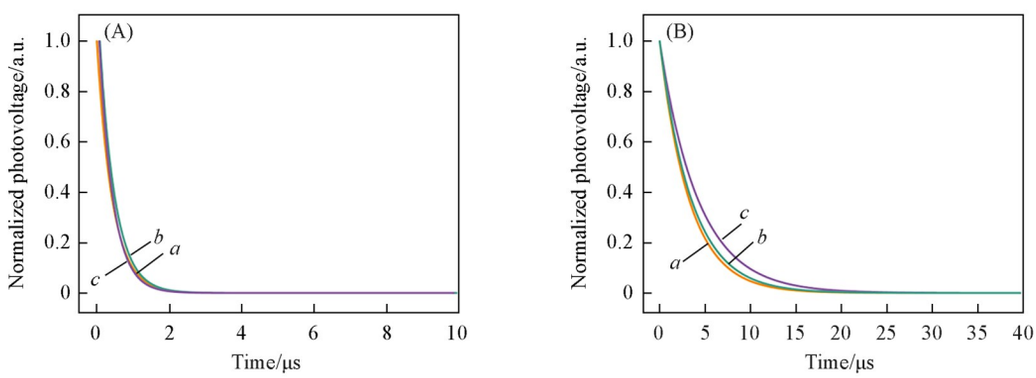

Fig. 6 TPC curves(A) and TPV curves(B) for the devices based on D18∶N3(*a*), D18∶N3∶BDT-C_2C_4(*b*) and D18∶N3∶BDT-C_8(*c*)

The efficiency retention of the device was measured under continuous light aging conditions of the same intensity, as shown in Fig.7. Both ternary devices exhibited better performance retention than the binary device, with a significantly lower PCE decay rate. Compared with the T_{80} lifetime (the time required to reach 80% of initial PCEs) of the D18∶N3 binary system (approximately 60 h), the T_{80} lifetimes of the devices based on D18∶N3∶BDT-C_2C_4 and D18∶N3∶BDT-C_8 were approximately 90 h and 120 h, respectively. The result indicated that the introduction of BDT-C_2C_4 or BDT-C_8 as the third component into the D18∶N3 binary system significantly improved the long-term stability of the devices under light irradiation.

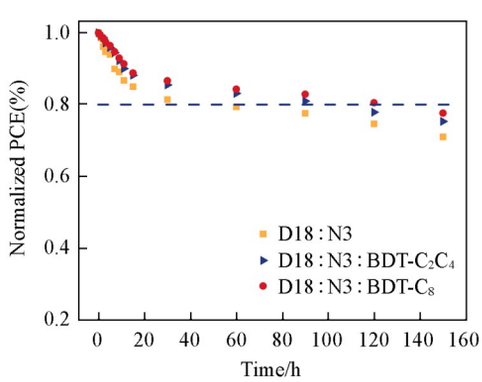

Fig. 7 Light stability of the devices

4 Conclusions

In summary, two "bridging" polymer acceptors (PAs), BDT-C_2C_4 and BDT-C_8, featuring a D-A-type backbone that structurally bridges the donor D18 and the SMA N3, were successfully designed and synthesized. These PAs not only filled the absorption gap between D18 and N3, but also presented well-aligned energy

levels. Incorporating these PAs as third components into the D18∶N3 blend suppressed the large phase separation, especially for the BDT-C8, showing good compatibility with both donor and SMA. The resulting optimized morphology, characterized by an interpenetrating fibrous network, facilitates exciton dissociation and charge transport. With the balanced hole/electron mobility, fastest extraction, and longest carrier lifetime, the ternary device based on D18∶N3∶BDT-C_8 blend achieved a champion PCE of 18.18% with simultaneously improved V_{OC}, J_{SC}, and FF. This work provides valuable insights for optimizing active layer morphology in high-performance ternary OSCs.

The supporting information of this paper see http://www.cjcu.jlu.edu.cn/CN/10.7503/cjcu20250324.

References

[1] Bi X., Li S., He T., Chen H., Li Y., Jia X., Cao X., Guo Y., Yang Y., Ma W., Yao Z., Kan B., Li C., Wan X., Chen Y., *Small*, **2024**, *20*(24), 2311561
[2] Deng M., Xu X., Duan Y., Qiu W., Yu L., Li R., Peng Q., *Adv. Mater.*, **2023**, *36*(11), 2308216
[3] Guo Y., Chen Z., Ge J., Zhu J., Zhang J., Meng Y., Ye Q., Wang S., Chen F., Ma W., Ge Z., *Adv. Funct. Mater.*, **2023**, *33*(47), 2305611
[4] Hu H., Liu S., Xu J., Ma R., Peng Z., Peña T. A. D., Cui Y., Liang W., Zhou X., Luo S., Yu H., Li M., Wu J., Chen S., Li G., Chen Y., *Angew. Chem. Int. Ed.*, **2024**, *63*(15), e202400086
[5] Liang W., Chen L., Wang Z., Peng Z., Zhu L., Kwok C. H., Yu H., Xiong W., Li T., Zhang Z., Wang Y., Liao Y., Zhang G., Hu H., Chen Y., *Adv. Energy Mater.*, **2024**, *14*(11), 2303661
[6] Su Z., Liu W., Lin Y., Ma Z., Zhang A., Lu H., Xu X., Li C., Liu Y., Bo Z., *Small*, **2024**, *20*(35), 2310028
[7] Tao J., Yang K., Qiu D., Wang C., Zhang H., Lv M., Zhang J., Lu K., Wei Z., *Nano Energy*, **2024**, *125*, 109540
[8] Wang T., Wang W., Cui Y., Ren J., Chen Z., Wang J., Li H., Li J., Hou J., *Adv. Funct. Mater.*, **2024**, *34*(34), 2400729
[9] Yang C., Zhan S., Li Q., Wu Y., Jia X., Li C., Liu K., Qu S., Wang Z., Wang Z., *Nano Energy*, **2022**, *98*, 107299
[10] Zhou K., Wu Y., Liu Y., Zhou X., Zhang L., Ma W., *ACS Energy Lett.*, **2019**, *4*(5), 1057—1064
[11] Chen P. Y., Zhang G. Y., Li J. G., Ma L. J., Zhou J. Y., Zhu M. G., Li S., Wang Z., *Chem. Res. Chinese Universities*, **2024**, *40*(2), 293—304
[12] Fu J., Fong P. W. K., Liu H., Huang C. S., Lu X., Lu S., Abdelsamie M., Kodalle T., Sutter-Fella C.M., Yang Y., Li G., *Nat. Commun.*, **2023**, *14*(1), 1760
[13] Gillett A. J., Privitera A., Dilmurat R., Karki A., Qian D., Pershin A., Londi G., Myers W. K., Lee J., Yuan J., Ko S. J., Riede M. K., Gao F., Bazan G. C., Rao A., Nguyen T. Q., Beljonne D., Friend R. H., *Nature*, **2021**, *597*(7878), 666—671
[14] Xia H., You C., Fu J., Luo D., Ma R., Liu H., Lang Y., Lu X., Zhu W., Li G., *Adv. Mater.*, **2025**, *37*(37), 2501428
[15] Sun Z. H., Yin P. P., He S. Y., Zhang K. G., Pan X. R., Wang J. Y., Hao P. N., Zhou Z., Yang X. G., Ma L. F., Tan C. L., *Chem. Res. Chinese Universities*, **2025**, *41*(3), 519—524
[16] Bai H., Fan Q., Ma R., Guo X., Ma W., Zhang M., *Chin. J. Chem.*, **2024**, *42*(11), 1307—1318
[17] Liu Q., Jiang Y., Jin K., Qin J., Xu J., Li W., Xiong J., Liu J., Xiao Z., Sun K., Yang S., Zhang X., Ding L., *Sci. Bull.*, **2020**, *65*(4), 272—275
[18] Yuan J., Zhang Y., Zhou L., Zhang G., Yip H. L., Lau T. K., Lu X., Zhu C., Peng H., Johnson P. A., Leclerc M., Cao Y., Ulanski J., Li Y., Zou Y., *Joule*, **2019**, *3*(4), 1140—1151
[19] Chen Z., Zhu J., Yang D., Song W., Shi J., Ge J., Guo Y., Tong X., Chen F., Ge Z., *Energy Environ. Sci.*, **2023**, *16*(7), 3119—3127
[20] Sun F., Wu J., Cheng B., Kan L., Hua F., Sun W., Wang H., Huo Y., Chen S., Xia X., Du X., Liu F., Wang E., Guo X., Li Y., Zhang M., *Energy Environ. Sci.*, **2025**, *18*(14), 7071—7081
[21] Wang Y., Yu H., Zhao D., Liu W., Liu B., Wu X., Gao D., Zhang D., Zhang S., Sun X., Zhang C., Zhao C., Fu Y., Song W., Gong S., Fu Y., Kwok C.H., Ge Z., Lu X., Chen X., Xiao S., Wong W.Y., Chai Y., Yan H., Zhu Z., *Adv. Energy Mater.*, **2025**, *15*, 2404499
[22] Wei Y., Zhou X., Cai Y., Li Y., Wang S., Fu Z., Sun R., Yu N., Li C., Huang K., Bi Z., Zhang X., Zhou Y., Hao X., Min J., Tang Z., Ma W., Sun Y., Huang H., *Adv. Mater.*, **2024**, *36*(28), 2403294
[23] Lee J. W., Sun C., Lee J., Kim D. J., Kang W. J., Lee S., Kim D., Park J., Phan T. N. L., Tan Z., Kim F. S., Lee J. Y., Bao X., Kim T. S., Kim Y. H., Kim B. J., *Adv. Energy Mater.*, **2024**, *14*(8), 2303872
[24] Liang Q., Jiao X., Yan Y., Xie Z., Lu G., Liu J., Han Y., *Adv. Funct. Mater.*, **2019**, *29*(47), 1807591
[25] Ma R., Fan Q., Dela Peña T.A., Wu B., Liu H., Wu Q., Wei Q., Wu J., Lu X., Li M., Ma W., Li G., *Adv. Mater.*, **2023**, *35*(18), 2212275
[26] Li M., Zhang F., Chen Y., Liu Y., Wang D., Shen Z., Zhao J., Xu D., Li X., *J. Energy Chem.*, **2025**, *110*, 864—872

[27] Li Z., Zhao H., Li H., Xie J., Zhao J., Liu L., Yang Z., Dou Y., Dong M., Zhang K., Huang F., *J. Mater. Chem. A*, **2025**, *13*(33), 27082—27092
[28] Wang P., Bi F., Jiang H., Wang X., Cui C., Li Y., Bao X., *Adv. Funct. Mater.*, **2024**, *35*(1), 2411862
[29] Zhao F., Wang C., Zhan X., *Adv. Energy Mater.*, **2018**, *8*(28), 1703147
[30] Zhou R., Jiang Z., Shi Y., Wu Q., Yang C., Zhang J., Lu K., Wei Z., *Adv. Funct. Mater.*, **2020**, *30*(51), 2005426
[31] Zou B., Wu W., Dela Peña T.A., Ma R., Luo Y., Hai Y., Xie X., Li M., Luo Z., Wu J., Yang C., Li G., Yan H., *Nano-Micro Lett.*, **2023**, *16*, 30
[32] Chen Q., Wang W., Liu X., Iqbal S., Wang Z., *Renew. Sust. Energy Rev.*, **2025**, *216*, 115673
[33] Doumon N. Y., Yang L., Rosei F., *Nano Energy*, **2022**, *94*, 106915
[34] Wang S., Wang L., Zhang J., Gao H., Xiao M., Song H., *Nano Energy*, **2025**, *143*, 111329
[35] Zhang L., Xu X., Lin B., Zhao H., Li T., Xin J., Bi Z., Qiu G., Guo S., Zhou K., Zhan X., Ma W., *Adv. Mater.*, **2018**, *30*(51), 1805041
[36] Hu H., Zhang R., Jiang D., Mu X., Yi J., Yu H., Ma L. K., Li B., Cao L., Sha M., Sun J., Gui R., Liu W., Liang S., Li L., Huang S., Yuan J., Niu C., Qu C., Yuan J., Zhou R., Zhang C., Lu L., Du X., Gao K., Li W., So S. K., Zou Y., Sun Y., Hao X., Gao F., Yan H., Yin H., *Nat. Commun.*, **2025**, *16*(1), 6546
[37] Rivnay J., Jimison L. H., Northrup J. E., Toney M. F., Noriega R., Lu S., Marks T. J., Facchetti A., Salleo A., *Nat. Mater.*, **2009**, *8*, 952—958
[38] Chen J., Wu Y., Chen L., Liao Y., Zhu Y., Saparbaev A., Wan M., Wu J., Li Y., Xiang H., Saidkulova A., Wang X., Yang R., *Adv. Funct. Mater.*, **2025**, *35*(49), e08397
[39] Liang W., Zhu S., Sun K., Hai J., Cui Y., Gao C., Li W., Wu Z., Zhang G., Hu H., *Adv. Funct. Mater.*, **2024**, *35*(7), 2415499
[40] Zhang Y., Liu R. R., Zhang B. Y., Chen X., Zhang Y. H., Wang C. L., Zhang H. L., *J. Mater. Chem. A*, **2025**, (3), 39271—39278

(Ed.: W, K, M)